WARSAW UNIVERSITY OF TECHNOLOGY Index 351733
FACULTY OF CIVIL ENGINEERING
COMMITTEE FOR CIVIL AND WATER ENGINEERING
POLISH ACADEMY OF SCIENCES ISSN 1230-2945

DOI: 10.24425/ace.2023.144182

ARCHIVES OF CIVIL ENGINEERING

Vol. LXIX ISSUE 1 2023

pp. 437 –451

Research paper

Experiment of the monitoring prestress loss of prestressed concrete beams with damages under static loading

Jinbo Wang[1], Guodong Li[2], Chunguang Lan[3], Nan Guo[4]

Abstract: In this paper, based on the feasible method and sensors for the full-scale prestressed monitor, the novel optical fiber sensors and the traditional monitoring sensors will be set up into two prestressed concrete beams with the same geometrical dimensions, material properties, and construction conditions, etc. to investigate the working state of the novel sensors and obtain the evolution law of prestress loss of the prestressed feature component under the static load. The results show that the evolution law of prestress loss of the loaded beam under the condition of no damage state and initial crack is the same as the non-loaded one; however, the prestress loss increases with the increase of time under the situation with the limit crack. The total loss of the prestressed beam with the limit crack is 36.4% without damage. The prestress loss of the prestressed beam under the static load increase with the development of the crack (injury).

Keywords: optical fiber Bragg grating, optical fiber sensing technology, prestress loss, prestressed concrete beam, smart steel strand

[1]M.E., Northeast Forestry University, School of Civil Engineering, A1. Harbin City, Heilongjiang Province, China, e-mail: 33831705@qq.com, ORCID: 0000-0002-3637-187X

[2]Prof., PhD., Northeast Forestry University, School of Civil Engineering, A1. Harbin City, Heilongjiang Province, China, e-mail: ldlgd@163.com, ORCID: 0000-0002-4827-7493

[3]PhD., Beijing Building Construction Research Institute Co., Ltd, A1. Beijing, China, e-mail: lcg98011210@163.com, ORCID: 0000-0002-9989-6112

[4]Prof., PhD., Northeast Forestry University, School of Civil Engineering, Al. Harbin City, Heilongjiang Province, China, e-mail: snowguonan@163.com, ORCID: 0000-0003-4790-0818

1. Introduction

The prestressed concrete structure evolved from the reinforced concrete structure. Prestressed concrete technology was first widely used in European countries to solve the problem of the shortage of steel required for reconstruction after World War II, and then developed rapidly all over the world [1]. Beam-type prestressed concrete structural members are the most widely used among these structural forms of prestressed concrete structures, especially in bridge engineering. Since the end of the 20th century, more than 70% of the bridges built around the world have adopted prestressed concrete structures [2,3]. The prestress loss is defined as the phenomenon that during the long-term service period of the prestressed concrete structural members, the tensile stress of the prestressed tendon will continue to decrease from the construction of the member to the end of the service life [4–7]. The occurrence of prestress loss inevitably produces the resistance attenuation of prestressed concrete structural members, which reduces the normal function of the structure and the ability to resist natural disasters, and even leads to catastrophic consequences. The engineering community has reached a consensus: at the end of the service period of prestressed concrete structure, the long-term prestress loss caused by overload, material performance degradation, harsh service environment, and other factors will lead to the expansion of cracks, which will intensify water erosion, corrosion deterioration, and the resistance of prestressed structures will be severely degraded. Nearly 10,000 small prestressed beam bridges were built in China at the end of the 20th century with a wide range of crack expansion problems. Their safety assessment and bearing capacity calculation had no basis because of the inability to get the prestressed state of steel bars or steel strands, which has become an astriction of engineering worldwide [8–16]. Therefore, analyzing the evolution law of prestress loss in different damage stages of prestressed concrete beams under static load is essential.

Because of the need for monitoring the prestress loss in the damaged state of prestressed concrete structures, this paper comprehensively considers the characteristics of fiber Brillouin sensing technology and fiber grating sensing technology. It then puts forward a prestress loss monitoring method based on fiber Brillouin sensing technology and fiber Bragg grating sensing technology and develops a smart steel strand to meet the practical application of engineering. On this basis, the new optical fiber smart steel strand and the traditional prestress loss monitoring sensor are simultaneously arranged in two prestressed concrete beams under the same conditions. The evolution law of prestress loss in different damage states of prestressed concrete beams under static load is obtained, then compared with the non-loaded beam, which can provide data support for the design method and safety evaluation of prestressed concrete beams.

2. The monitoring method of prestress loss which is based on optical fiber sensing technology

According to the generation mechanism of the prestress loss, it can be known that the prestress loss is time-variable and closely related to the spatial position. We choose a method based on the Brillouin optical time-domain analyzer (BOTDA) and the quasi-distributed

fiber Bragg grating (FBG) array as a supplement (to solve the problems of boundary effect and low sampling frequency of BOTDA) to obtain the time and space distribution information of prestress loss to accurately obtain prestress loss states of prestressed steel bars in fully distributed prestressed concrete structures (Figure 1).

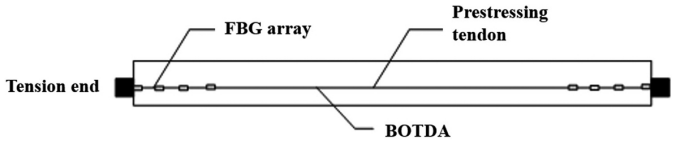

Fig. 1. Schematic diagram of the full-scale prestress loss monitoring method

In consideration of the characteristics of fiber Brillouin strain sensors and fiber Bragg grating strain sensors, the practical stress values of steel strands obtained by the fiber sensor are as follows:

$$\sigma = \frac{E_{IC}}{k_{\varepsilon}} \Delta_{v} \tag{2.1}$$

$$\sigma = \frac{E_{IC}}{\alpha_{\varepsilon}} \Delta_{\lambda_{\beta}} \tag{2.2}$$

where: $\Delta\lambda_B$ – the central wavelength change value of the fiber Bragg grating (nm), α_ε – the sensitivity coefficient of the relationship between the axial strain of fiber Bragg grating and the change of central wavelength(nm), Δv_B – the drift value of the Brillouin scattering frequency before and after the fiber is strained (Hz), k_ε – the sensitivity coefficient of the relationship between optical fiber axial strain and optical frequency drift value (Hz).

3. Optical fiber smart steel strand

3.1. Fundamental

The reinforced Fiber Brillouin smart rebar and the fiber Bragg grating smart rebar are designed and manufactured to meet the needs of prestress loss monitoring of prestressed concrete structures. Then the smart rebars are used to replace the medium core wire of conventional 7-wire smart steel strand to assemble a new type of smart steel strand (Figure 2).

In order to ensure the synergistic deformation of the smart rebar and the outer wire of the ordinary steel strand, several layers of high-ductility metal sheets (the 0.02 mm copper foil is used in this study) are wrapped on the surface of the smart rebar, the interlayer friction between the smart rebar and the outer wire of ordinary steel strand is improved by increasing the diameter of the smart rebar. With the help of the steel strand's end anchoring and torsion effect under stress, the smart rebars will be naturally wrapped to make the effect of synergistic deformation [17–20].

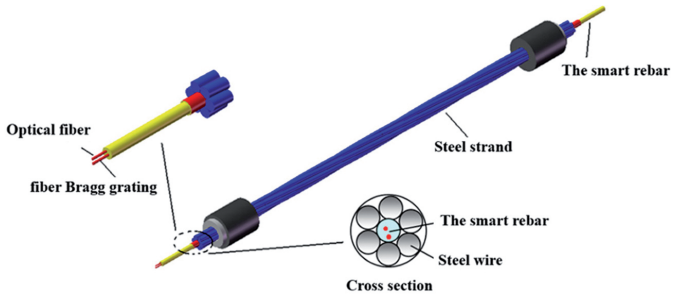

Fig. 2. The smart steel strand

3.2. Calibration test

In order to verify the sensing performance of the fiber Bragg grating sensor in the smart steel strand, the following calibration tests are carried out. The experimental subject is a 3 meters smart steel strand; the loading equipment of the test is a jack and a reaction frame; the fiber grating sensor demodulator is Si720 of the American MOI Company; the loading method is step-by-step loading with 20 kN as a level. After reaching 200 kN, unload to a powerless state with the same series, and repeat five cycles. The test device and results are shown in Fig. 3 and Fig. 4, respectively. The calibration test results show that the tensioning and anchoring tools of the traditional prestressed steel bar could be used for the smart steel strands; the linearity and repeatability of the test results are pretty good, and the linear fitting coefficient is $n = 99.993\%$.

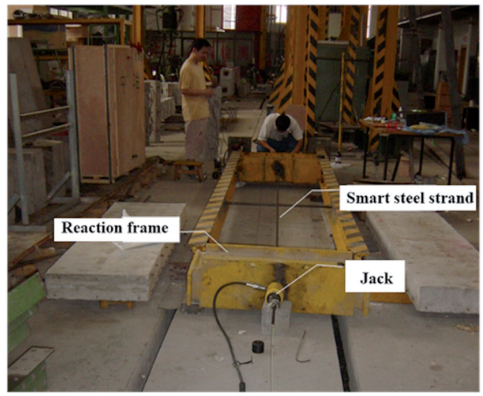

Fig. 3. Calibration device of fiber Bragg grating sensor in the smart steel strand

In order to verify the strain sensing characteristics of the optical fiber Brillouin sensor in the smart steel strand, the following calibration test is specially made. The experimental subject is a 3 m long smart steel strand which is the same as the fiber grating sensor calibration test; The loading device is a 100 kN manual hydraulic jack and a self-made horizontal tensile machine; The maximum load of the test is 30 kN, and the total load value

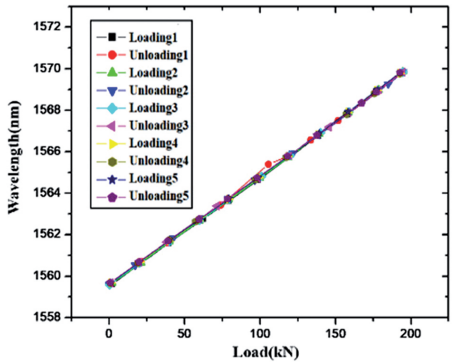

Fig. 4. Test results of the calibration

is applied in nine stages during the test; the fiber Brillouin frequency shift demodulator is the DiTeSt Brillouin optical time-domain analyzer (BOTDA) produced by OMNI, Switzerland. The minimum spatial resolution is 10 cm, and the strain measurement accuracy is 20 $\mu\varepsilon$; The gauge distance of the extensometer is 50 mm, which is arranged in the middle of the smart steel strand. The test device is shown in Fig. 5. Figure 6 is a diagram showing the

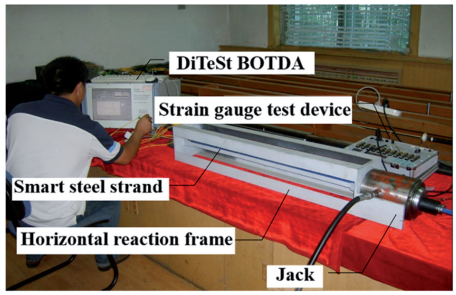

Fig. 5. Strain sensing test of fiber optic Brillouin smart Steel strand

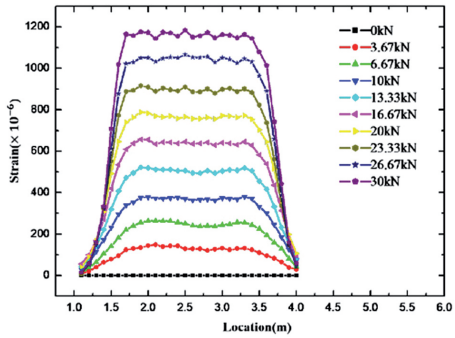

Fig. 6. The strain distribution pattern along the smart steel strand

spatial distribution of the strain of the steel strand measured by the optical fiber Brillouin sensor, and Fig. 7 is a comparison diagram of the strain test by BOTDA at the corresponding position and the strain test by the extensometer. It can be seen from Fig. 6 that the smart steel strand test range is within the scope of 1÷4 m. Excluding the 0.5 m range affected by the end effect of the test method, the strains obtained at each point of the smart steel strand are equal and consistent with the theoretical results. It can be seen from Fig. 7 that the strain measured by the optical fiber Brillouin sensor in the smart steel strand is consistent with the test data of the extensometer, and the error is less than 2%.

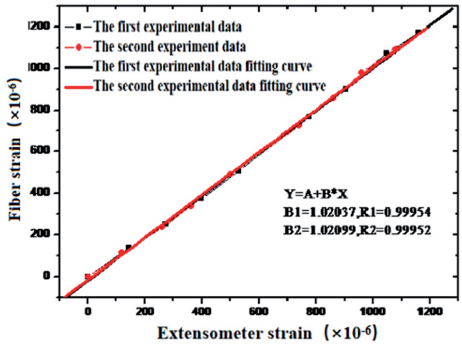

Fig. 7. Comparison of the strain between the extensometer and the smart steel strand in the same position

4. Prestress loss monitoring test of prestressed concrete beams in a damaged state

4.1. Test overview

4.1.1. Test beam design

In order to meet the needs of comparative analysis, the test samples are two prestressed concrete beams with the same conditions (material, geometry, construction conditions, etc.); the beam section size is 100 mm × 200 mm, and the span is 3 m, and a straight channel with a diameter of 30 mm is reserved; The prestressed reinforcement is equipped with a single smart steel strand. The nominal diameter of the smart steel strand is 15.12 mm, and the standard strength value is 1660 MPa; The grade of concrete is C40; The non-prestressed steel bars are of HRB335, and 2Φ10 are arranged in the tension zone, and the compression zone of the test beam respectively; The hooping are Φ6@200. The schematic diagram of the test beam is shown in Fig. 8. No finished corrugated pipe can be used directly because of the small section size of the test beam. Therefore the test beam adopts a PVC pipe with a diameter of 30 mm to form holes. The tensioning and anchoring end is pre-embedded with steel backing plates and spiral bars to withstand local pressure. The

thickness of the steel backing plates is 10 mm, the diameter of the spiral bars is 4 mm, the inner diameter is 50 mm, and there are five turns.

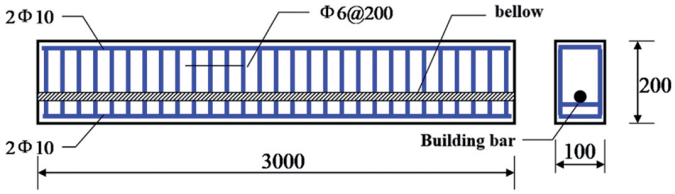

Fig. 8. Geometric dimension of the test beam

4.1.2. Sensor system

In order to investigate the evolution law of the prestress loss of the prestressed concrete beam in the damaged state, the sensor systems selected in this experiment are mainly the novel smart steel strand and the traditional pressure sensor. The smart steel strand includes a full-length fiber Brillouin sensor and a double fiber grating (located at the beam end and mid-span, respectively) collinear sensor. The pressure sensor is a 20-ton resistance strain pressure sensor arranged between the prestressed concrete beam anchor and the anchor plate. The schematic layout of the sensor system is shown in Fig. 9.

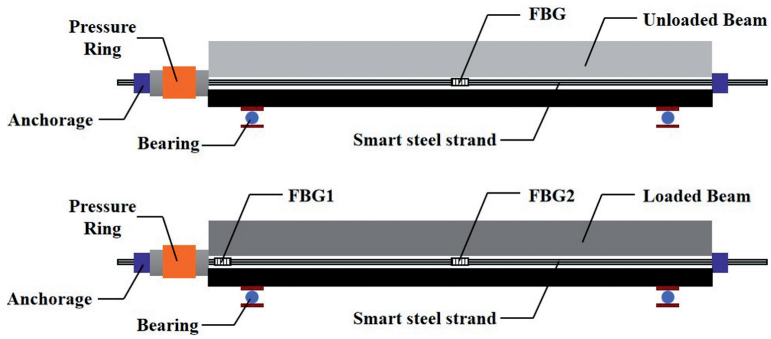

Fig. 9. Schematic diagram of test sensor system layout

4.1.3. Loading form

a) Application of prestressing

The prestressed steel bar is tensioned from one direction. The tensioning equipment is a standard single-hole top anchor prestressing tensioner, the tensioning control stress is about $\sigma_{con} = 0.7 f_{ptk}$ (the f_{ptk} of the smart steel strand is 1660 MPa), and the maximum tensioning load is about 160 kN. The tension is loaded in five stages, and the process is $0 \rightarrow$ straightening (about 6 kN) $\rightarrow 20\%\sigma_{con} \rightarrow 50\%\sigma_{con} \rightarrow 80\%\sigma_{con} \rightarrow 100\%\sigma_{con} \rightarrow$ releasing and anchoring.

b) Application process of the static load

Select one of the two test beams to apply a static load, and the other is stationary near the test stand. The loading position is 500 mm on the left and right of the mid-span of the beam. The loading is applied through the reaction frame and distribution beam by a 10-ton hydraulic jack. The loading is controlled by the resistance strain gauge pressure transducers mounted between the reaction frame and the jack. In order to eliminate the loss of prestress caused by the movement of the test beam, the loaded test beam does not move after being stretched on the test frame. The test stand and devices are shown in Figs. 10a and 10b.

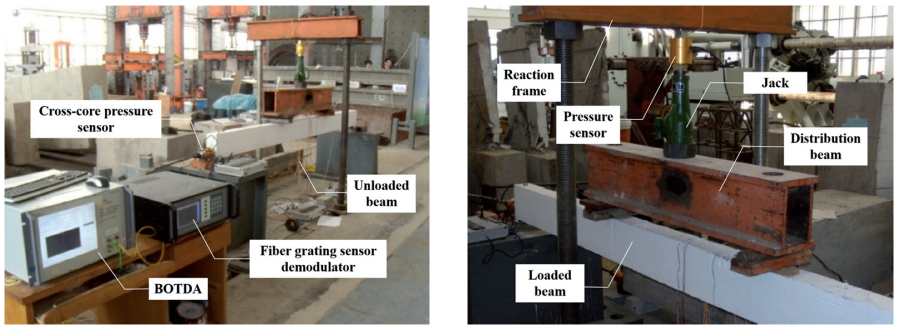

(a) (b)

Fig. 10. Test stand and devices: (a) Test stand, (b) Test devices

The experimental load shall be applied 20 days after the completion of prestressed concrete beam construction. The load is applied in several stages. In the early stage, apply 3 kN for each level of load. When the total load reached 9 kN, it was reduced to 1.5 kN per stage until the first crack appeared in the prestressed concrete beam, then the load could be unloaded and keep this state for ten days after the end; The load was unloaded until the maximum crack width of the prestressed concrete beam reached 0.2 mm, then keep this state for ten days.

4.1.4. Test data acquisition

In the construction process, the control load of each level and the reasonable time for stretch and anchor are selected (Principle of time point selection: The early stage will be dense and the later stage will be loose), and collect the data measured by all sensors in the test beams simultaneously (Including fiber grating sensors, optical fiber sensors, resistance strain pressure sensors, etc. in smart steel strands). The center wavelength of the fiber grating sensor is collected by the Si720 demodulator produced by MOI Company in the United States, and the light wave frequency shift value of the fiber Brillouin sensor is collected by the DiTeSt series Brillouin optical time-domain analyzer (BOTDA) produced by OMNI Co., Ltd. in Switzerland. The resistance strain pressure sensor adopts the static strain gauge produced by Donghua Instrument and Meter Factory.

4.2. Test Results and Analysis

4.2.1. Prestressing stage

Figure 11 shows the test results of the fiber grating sensor in the smart steel strand during the construction phase. The figure's non-loaded and loaded beams represent the prestressed concrete beam with no and static load in the subsequent test, respectively. It can be seen from the figure that the central wavelength value of the fiber grating sensor increases linearly with the increase of the load. The fiber Bragg grating sensor in the two beams has a similar sensitivity coefficient, which indicates that the two beams are used to compare and investigate the prestress state of the prestressed reinforcement under different damage conditions is feasible.

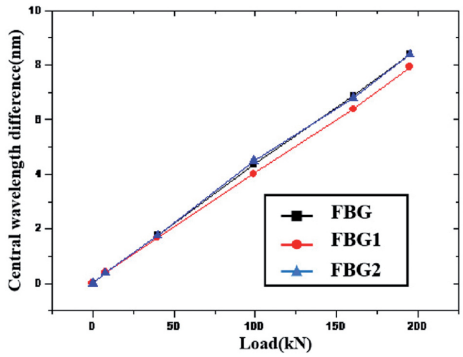

Fig. 11. Test results of fiber Bragg grating sensor in smart steel strand during the construction stage

Similarly, in order to investigate the working condition of the optical fiber Brillouin sensor in the smart steel strand, The variation law of the data measured by the fiber optic Brillouin sensor during the construction phase is drawn, as shown in Fig. 12. During the test, in order to save the number of BOTDA channels and test time, and to give full play to the advantages of distributed measurement of fiber Brillouin sensing technology, the test data will be collected simultaneously after connecting the optical fiber sensors in the loaded beam and the non-loaded beam in series. In Figs. 12a and 12c, the test range of the smart steel strand in the loaded beam (the range from 5 m to 8 m on the x-axis in the figure) and the non-loaded beam (The range from 13 m to 16m on the x-axis in the figure) can be distinguished. Fig. 12b and 12d are the graphs of the variation of strand strain with load at the midpoint of the non-loaded and loaded beams, respectively. (Point A is the midpoint of the span of the unloaded beam – 6 m from the test area, and Point B is the midpoint of the span of the loaded beam – 15 m from the test area) It can be seen from the figure that the strain of the steel strand increases linearly with the increase of the load during the construction process. The test sensitivity coefficients of the fiber-optic Brillouin sensor in the two beams are relatively close, and their values are 40.6 $\mu\varepsilon$/kN and 37.6 $\mu\varepsilon$/kN, respectively. This further shows that it is feasible to study the stress state of prestressed steel

bars under different damage conditions by using the comparative test method of fiber-optic Brillouin sensors in two prestressed concrete beams.

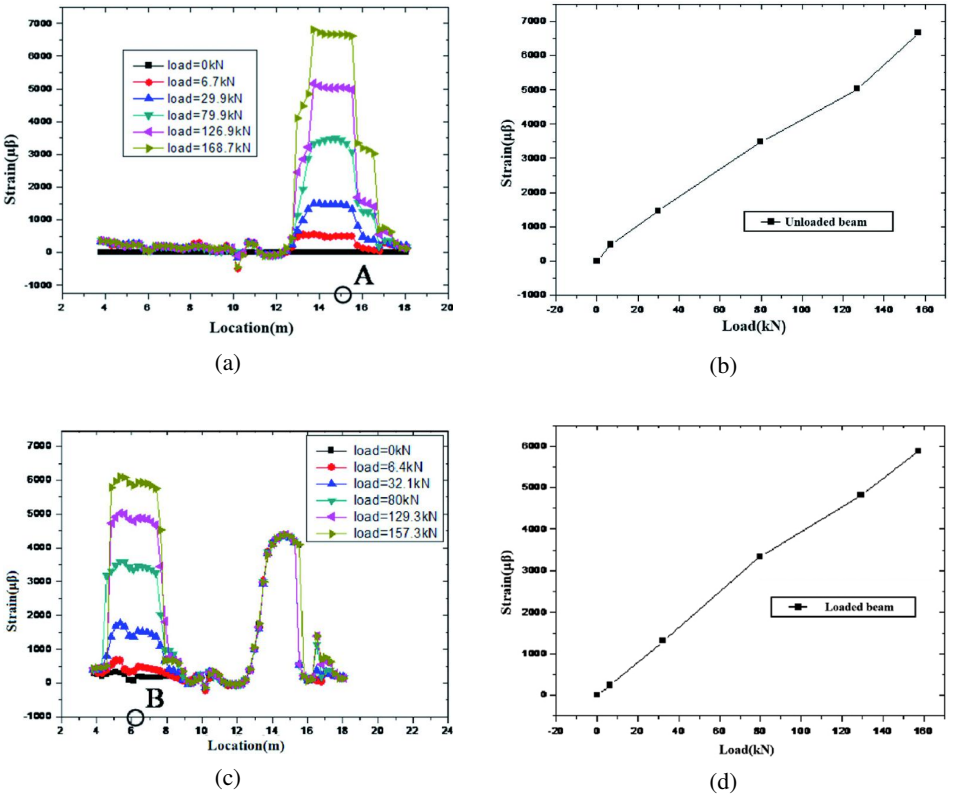

Fig. 12. Optical fiber Brillouin sensor test data during the construction phase: (a) Data during the non-loaded beam is in tension, (b) Point A, (c) Data during the loaded beam is in tension, (d) Point B

4.2.2. Damage-free state

In order to investigate the test validity of the fiber grating sensor in the smart steel strand and obtain the evolution law of the prestress loss in the non-damaged state, the test data of the fiber grating sensor was compared with the test results of the traditional resistance strain pressure sensor, as shown in Fig. 13. It can be seen from the figure that the evolution law of the prestress loss measured by the resistance strain pressure sensor is consistent with the test result of the fiber grating sensor. The prestress loss of the prestressed concrete beam in the non-damaged state increases with the growth of time, and the change is significant in the first two days and then gradually decreases. The prestress loss of the test beam is about 36 MPa at about 20 days.

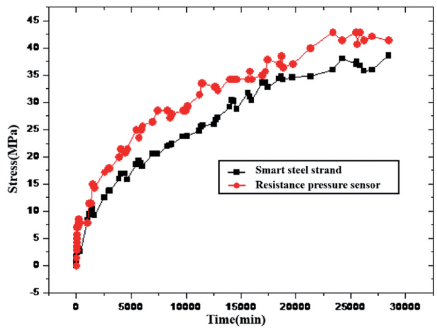

Fig. 13. Prestress loss measured based on smart steel strand and pressure sensor

4.2.3. Unloading stage after the initial crack of prestressed concrete beam

In order to investigate the prestress loss in the initial cracking state of prestressed concrete beams, smart strands were used to obtain the evolution law of prestress loss in loaded and unloaded beams after the initial cracking of loaded beams was unloaded to no load, which is plotted within Fig. 14. It can be seen from the figure that the evolution law curves of the prestress loss of the two beams are approximately horizontal, which shows that the initial crack damage under static load does not affect the prestress loss. The reason is that in the initial stage of concrete cracking, the concrete beam is only slightly damaged (only one or two visible cracks), and the cracks are all closed after unloading, which has little effect on the stress of the prestressed tendons. Therefore, the prestress loss value of the prestressed steel bar caused by the unloading state after the initial crack could be ignored.

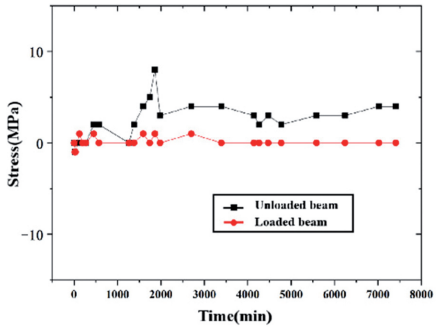

Fig. 14. Comparison of variation law of prestress loss in the unloading stage after initial cracking

4.2.4. After the cracks in the prestressed concrete beams reach the limit

After completing the collection of long-term prestress loss in the unloading stage after initial cracking, continue to apply loads to the loaded beams gradually according to the load levels specified in the loading history. With the continuous increase of the external load,

the cracks of the prestressed concrete loaded beam slowly appeared and became denser in the pure bending section. When the load reached 50 kN, the maximum crack width of the lower edge of the prestressed concrete beam reached 0.2 mm. The crack distribution and width of the test beams are shown in Fig. 15. After unloading the beam to no-load, the optical fiber sensor and fiber grating sensor in the smart steel strand is used to obtain the evolution law of the prestress loss of the loaded beam and the non-loaded beam.

(a) (b)

Fig. 15. Distribution and measurement of cracks in prestressed concrete: (a) Crack distribution and (b) Crack measurement

Figure 16 is a three-dimensional stress nephogram based on the test data of the optical fiber in the smart steel strand and plotted with time and position as axes. It can be seen from the figure that the prestress loss of prestressed steel bars is unevenly distributed along the beam length direction. The prestress loss of the section at the 6 m and 7 m positions is more significant, and the other positions are relatively more minor. It can be seen from the loading scheme of the test beam and the arrangement of the optical fiber Brillouin sensor that the 6 m position and 7 m position on the drawing are the two loading points

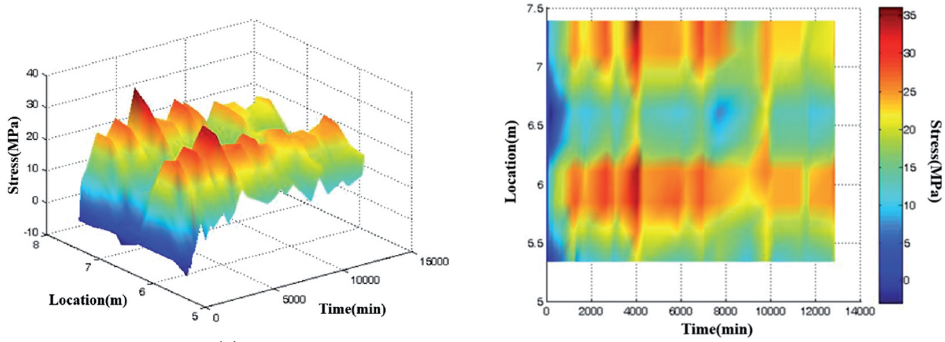

(a) (b)

Fig. 16. Prestress loss measured by Optical fiber Brillouin sensor: (a) Graphic model and (b) Stress nephogram

of four-point bending. According to the test phenomenon, the prestressed concrete beam has more and wider cracks at these two points. Therefore, it shows that the prestress loss of prestressed steel bars in the beam section is related to the distribution of cracks on this beam, that is, the more concentrated the cracks are, the greater the prestress loss of prestressed reinforcement is.

Figure 17 shows the evolution law of prestress loss measured by fiber Bragg grating sensors of loaded and unloaded beams after the crack reaches the limit value. It can be seen from the figure that the prestress loss of the non-loaded beam remains stable with the continuous growth of time after the prestressed concrete beam reaches the crack limit and is unloaded. The prestress loss of the corresponding loaded beam increases significantly. The final loss value is about 12 MPa, accounting for 33.3% of the prestress loss in the undamaged state. It shows that the state of crack reaching the limit obviously weakens the stress of prestressed reinforcement of prestressed concrete beam. The reason is that when the prestressed concrete beam comes to the crack limit, there are many cracks on the beam and the width is large, and the concrete has fallen off at some positions. After the load on the prestressed concrete beam is removed, the concrete beam is squeezed under the action of prestressing, which leads to the shortening of the anchorage length of the plane of prestressed reinforcement, and then leads to the loss of partial prestress.

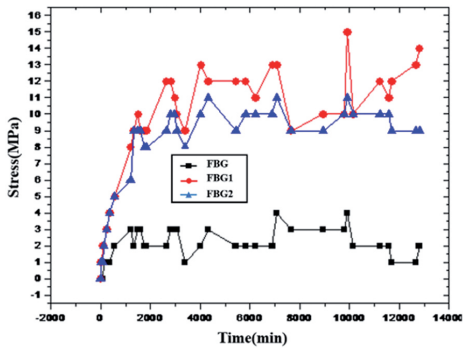

Fig. 17. Comparison diagram of prestressing loss when the crack reaches the limit value

4.2.5. Evolution law of prestress in the whole process of static loading

In order to investigate the influence of damage state on the prestress loss of prestressed concrete beam more intuitively, the test results of fiber Bragg grating sensor of the loaded beam and the non-loaded beam under no damage state, unloading state after the initial crack, and unloading state after the crack reaches the limit are drawn in this figure, as shown in Fig. 18. It can be seen from the figure that the prestress loss of the non-loaded prestressed concrete beam gradually increases with the growth of time, in which changes rapidly in the early stage, and then gradually tends to remain stable; At the same time, the prestress loss of the loaded prestressed concrete beams changes obviously with different damage states, and the variation law of prestress loss in non-damage state and unloading

state after initial crack is the same as that of non-loaded beams; After the crack reaches the limit value, the prestress loss of the loaded beam continue to increase and remains a stable value again. To sum up, the prestress loss of prestressed concrete beams increases with the increase of cracks, and the prestress loss caused by larger cracks can not be ignored.

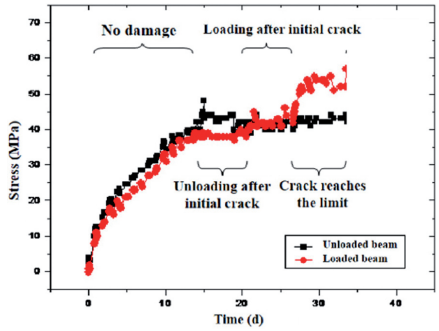

Fig. 18. Comparison of prestress loss of two beams

5. Conclusions

In this paper, the smart steel strand and the traditional prestress loss monitoring sensor are placed simultaneously in two prestressed concrete beams with the same conditions. The evolution law of prestress loss in each stage of the test beam from static load to failure is compared and analyzed by applying static load to one of the prestressed concrete beams. The conclusions are as follows:

1. The smart steel strand can adopt the same layout scheme, tensioning instrument, and anchoring equipment as the ordinary steel strand, and the construction is simple and convenient; The evolution law of prestress in each stage of the beam can be accurately obtained through the fiber optic sensor and fiber Bragg grating sensor in the smart steel strand; Compared with the traditional monitoring sensor, the accuracy is the same, but the stability, survival rate, test frequency, cost and impact on the original structure are superior.
2. The full-scale evolution law of prestressed concrete beams under static load can be accurately obtained using the smart steel strand. The performance of prestress loss in each stage is as follows: when there is no external force, the prestress loss gradually increases with time. In the early stage (1÷2 days), the rate is fast and progressively tends to be flat. At about 20 days, the long-term loss of prestressing is 36 Mpa; In the state of static load (unloading after the initial crack and crack reaching the limit value), the prestress loss changes with the distribution of beam cracks, that is, the greater the density and width of beam cracks, the more significant the prestress loss is, and when the cracks reach the limit value, the prestress loss at the stage increases to 12 MPa. It shows that the prestress loss caused by structural damage after the crack runs the limit value cannot be ignored.

References

[1] D.H. Cheng and Z.C. Xue, *Prestressed concrete structure*. Beijing, China: China Metrology Press, 2010.

[2] Y.P. Song, *Prestressed concrete bridge structure*. Dalian City, Liaoning Province, China: Machinery Industry Press, 2007.

[3] T.M. Ahlborn, C.K. Shield, and C.E. French, "Full-scale testing of prestressed concrete bridge girders", *Experimental Techniques*, vol. 21, pp. 33–35, 1997.

[4] X.C. Lao, T.H. He, L.Q. Tang, et al., "Pre-stress lose calculation and analysis of long span bridge base on monitoring of strain", *Journal of Experimental Mechanics*, vol. 21, pp. 742–746, 2006.

[5] S.H. Kim, S.Y. Park, S.T. Kim, and S.J. Jeon, "Analysis of Short-Term Prestress Losses in Post-tensioned Structures Using Smart Strands", *International Journal of Concrete Structures and Materials*, vol. 16, pp. 1–15, 2022, DOI: 10.1186/S40069-021-00488-3.

[6] P.M. Paez and B. Sensale, "Improved prediction of long-term prestress loss in unbonded prestressed concrete members", *Engineering Structures*, vol. 174, pp. 111–125, 2018, DOI: 10.1016/j.engstruct.2018.07.038.

[7] M. Boukendakdji, M. Touahmia, and M. Achour, "Comparative Study of Prestress Losses", *Engineering, Technology & Applied Science Research*, vol. 7, no. 3, pp. 1633–1637, 2017, DOI: 10.48084/etasr.1172.

[8] N. Guo, X.G. Wang, and C.G. Lan, "The technology and application of cable force monitoring for spatial cable structure", *Latin American Journal of Solids and Structures*, vol. 18, no. 8, pp. 1–10, 2021, DOI: 10.1590/1679-78256807.

[9] J. Janusz, "Fibre optic system based on FBG sensors for the monitoring of modern structures", *Archives of Civil Engineering*, vol. 68, no. 2, pp. 445–460, 2022, DOI: 10.24425/ace.2022.140652.

[10] V.D. Dao and V.H. Tran, "Research corrosion propagation time of reinforced concrete structures considering load influence", *Archives of Civil Engineering*, vol. 68, no. 2, pp. 563–576, 2022, DOI: 10.24425/ace.2022.140659.

[11] K. Mateja and K. Andrej, "Dynamic monitoring as a part of structural health monitoring of dams", *Archives of Civil Engineering*, vol. 68, no. 1, pp. 569–578, 2022, DOI: 10.24425/ace.2022.140186.

[12] Z.H. Ma and W. Hong, "Distributed displacement estimation of pre-stressed concrete beams with random cracks using long-gauge strain sensing", *Case Studies in Construction Materials*, vol. 17, pp. 1–10, 2022, DOI: 10.1016/J.CSCM.2022.E01296.

[13] S.T. Kim, Y.S. Park, C.H. Yoo, et al., "Analysis of Long-Term Prestress Loss in Prestressed Concrete (PC) Structures Using Fiber Bragg Grating (FBG) Sensor-Embedded PC Strands", *Applied Sciences*, vol. 11, no. 24, 2021, DOI: 10.3390/app112412153.

[14] Y.B. Lin, K.C. Chang, et al., "The health monitoring of a prestressed concrete beam by using fiber bragg grating sensors", *Smart Materials and Structures*, vol. 13, no. 4, pp. 712–718, 2004, DOI: 10.1088/0964-1726/13/4/008.

[15] J.H. Park, J.T. Kim, Y.S. Ryu, et al., "Monitoring cracks and prestress-loss in psc girder bridges using vibration-based damage detection techniques", in *Proceedings of 2007: SPIE Smart Structures and Materials + Nondestructive Evaluation and Health Monitoring*. 2007, DOI: 10.1117/12.720907.

[16] M. Przygocka and R. Kotynia, "Pre-stress losses in FRP pre-stressed reinforced concrete-subject overview", *Archives of Civil Engineering*, vol. 64, no. 4, pp. 257–268, 2018, DOI: 10.2478/ace-2018-0073.

[17] Y.P. Zhu and G.D. Chen, "Spiral Deployment of Optical Fiber Sensors for Distributed Strain Measurement in Seven-Wire Twisted Steel Cables, Post-Tensioned against Precast Concrete Bars", *Sensors*, vol. 22, no. 19, pp. 1–10, 2022, DOI: 10.3390/s22197636.

[18] C.G. Lan, H. Liu, and Z. Zhou, "Experimental investigation of prestress loss in PC beams based on BOTDA/FBG smart steel strands", *China Civil Engineering Journal*, vol. 46, no. 9, pp. 55–61, 2013, DOI: 10.15951/j.tmgcxb.2013.09.014.

[19] C.G. Lan, T.H. Wang, H. Liu, and J.P. Ou, "Development and application of fbg retard-bonded smart steel strands", *Journal of Harbin Institute of Technology*, vol. 46, no. 6, pp. 682–686, 2014, DOI: 10.11918/j.issn.0367-6234.2014.06.018.

[20] A.J. Hiba and G. Branko, "Monitoring of long-term prestress losses in prestressed concrete structures using fiber optic sensors", *Structural Health Monitoring*, vol. 18, no. 1, pp. 254–269, 2019, DOI: 10.1177/1475921717751870.

Received: 2022-08-24, Revised: 2022-11-29